



## Original Article

# Oxidation characteristics of porous-nickel prepared by powder metallurgy and cast-nickel at 1273 K in air for total oxidation time of 100 h



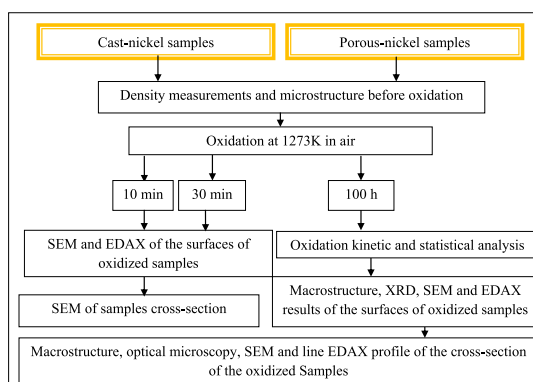
Lamiaa Z. Mohamed<sup>a,\*</sup>, Wafaa A. Ghanem<sup>b</sup>, Omayma A. El Kady<sup>c</sup>, Mohamed M. Lotfy<sup>a</sup>, Hafiz A. Ahmed<sup>a</sup>, Fawzi A. Elrefaie<sup>a</sup>

<sup>a</sup> Mining, Petroleum and Metallurgical Engineering Department, Faculty of Engineering, Cairo University, Egypt

<sup>b</sup> Corrosion and Surface Protection, Central Metallurgical Research and Development Institute (CMRDI), Helwan, Egypt

<sup>c</sup> Powder Technology Division, Central Metallurgical Research and Development Institute (CMRDI), Helwan, Egypt

## GRAPHICAL ABSTRACT



## ARTICLE INFO

## Article history:

Received 21 May 2017

Revised 15 August 2017

Accepted 17 August 2017

Available online 19 August 2017

## Keywords:

High temperature oxidation

Porous nickel

Cast nickel

Duplex macrostructure

Inward migration

Linear kinetics

## ABSTRACT

The oxidation behavior of two types of inhomogeneous nickel was investigated in air at 1273 K for a total oxidation time of 100 h. The two types were porous sintered-nickel and microstructurally inhomogeneous cast-nickel. The porous-nickel samples were fabricated by compacting Ni powder followed by sintering in vacuum at 1473 K for 2 h. The oxidation kinetics of the samples was determined gravimetrically. The topography and the cross-section microstructure of each oxidized sample were observed using optical and scanning electron microscopy. X-ray diffractometry and X-ray energy dispersive analysis were used to determine the nature of the formed oxide phases. The kinetic results revealed that the porous-nickel samples had higher trend for irreproducibility. The average oxidation rate for porous- and cast-nickel samples was initially rapid, and then decreased gradually to become linear. Linear rate constants were  $5.5 \times 10^{-8} \text{ g/cm}^2 \text{ s}$  and  $3.4 \times 10^{-8} \text{ g/cm}^2 \text{ s}$  for the porous- and cast-nickel samples, respectively. Initially a single-porous non-adherent NiO layer was noticed on the porous- and cast-nickel samples. After a longer time of oxidation, a non-adherent duplex NiO scale was formed. The two layers of the duplex scales were different in color. NiO particles were observed in most of the pores of the porous-nickel samples. Finally, the linear oxidation kinetics and the formation of porous non-adherent duplex oxide scales on the inhomogeneous nickel substrates demonstrated that the addition of new layers of

Peer review under responsibility of Cairo University.

\* Corresponding author.

E-mail address: [Lamiaa.zaky@cu.edu.eg](mailto:Lamiaa.zaky@cu.edu.eg) (L.Z. Mohamed).

<https://doi.org/10.1016/j.jare.2017.08.004>

2090-1232/© 2017 Production and hosting by Elsevier B.V. on behalf of Cairo University.

This is an open access article under the CC BY-NC-ND license (<http://creativecommons.org/licenses/by-nc-nd/4.0/>).

NiO occurred at the scale/metal interface due to the thermodynamically possible reaction between Ni and the molecular oxygen migrating inwardly.

© 2017 Production and hosting by Elsevier B.V. on behalf of Cairo University. This is an open access article under the CC BY-NC-ND license (<http://creativecommons.org/licenses/by-nc-nd/4.0/>).

## Introduction

Nickel is known to form only one oxide which exhibits a small range of non-stoichiometry,  $\text{Ni}_{1-x}\text{O}$ , this oxide behaves as a p-type semiconductor [1–3]. The oxidation status formed on Ni surfaces is studied by low energy bombardment using X-ray photoemission spectroscopy and secondary ion emission spectroscopy. The dominant nickel oxidation state is  $\text{Ni}^{2+}$  while some  $\text{Ni}^{3+}$  are present [4]. The oxidation of homogenous pure nickel substrates over the temperature range 700–1100 °C yields an adherent protective layer of nickel oxide [5,6]. In situ study for the oxidation behavior of nickel particles is carried out using environmental transmission electron microscope with 3.2 mbar of  $\text{O}_2$  between ambient temperature and 600 °C [7]. The kinetics of the oxide scale growth on the surface of non-porous homogenous nickel substrate and the scale characteristics are extensively studied [6,8–10]. Regardless of these extensive studies, discrepancies and important questions concerning nickel oxidation behavior are still to be answered [6].

At temperature over 1000 °C, the oxidation rate for homogenous nickel substrates is parabolic [5,6,11,12]. Thermogravimetric studies show that the oxidation process of sintered nickel green compacts in air at temperatures between 300 and 450 °C follows also a quadratic dependence on time [13]. For temperature ranging from 700 to 900 °C the oxidation rate is initially rapid. The rate then gradually decreases to become parabolic or continuously decreases [6,14]. The scale growth on homogenous nickel samples oxidized at temperatures over 1000 °C is controlled by cationic lattice diffusion; whereas, the short circuits diffusion of cations controls the scale growth at temperatures ranging from 700 to 900 °C [6].

When the temperature ranges from 900 to 1000 °C, the parabolic rate constants become widely distributed [15]. Several reasons were proposed for this phenomenon: metal purity [1], surface preparation [16], heat treatment [17] and the crystallographic orientation of nickel grains [18] modify the scale-growth rate dramatically [15]. A theoretical framework is devolved to provide an understanding of selected set of experimental finding of the oxidation process by single oxidant, this framework can be used as a predicted basis for oxidation rates under different conditions [19].

Under practical conditions, the protective oxide scales are exposed to internal stresses which cause loss of adherence, and consequently, duplex oxide scales are developed [5]. High temperature oxidation of inhomogeneous nickel might lead to formation of microfissures, transgranular crack propagation, porous oxide scales and cavity formation. Therefore, the oxide scales grow linearly by inward migration of molecular oxygen [6]. There are three main routes for the formation of microfissures and inward growth of NiO by migration of molecular oxygen: dissociation of the scale into pores and metal/oxide interface, stress-induced fissuring in the oxide scale and opening of microfissures as a consequence of differences in the rate of deformation across the growing oxide due to the inhomogeneity of the metal substrate [6].

Linear formation of NiO duplex scales is associated with inward migration of molecular oxygen [1,8,20–22]. The inner layer at the metal/scale interface is noticed to be consisting of small equiaxed grains overgrown by larger columnar grains in the external part; this type of scales is formed at temperature below 1000 °C [8].

Most of the nickel-based alloys might have inhomogeneous structure, and since limited systematic studies on the oxidation

behavior of inhomogeneous nickel and nickel-based alloys were carried out, the characteristics of the oxidation behavior of essential structural metals and alloys should be given a priority to determine the oxidation resistance of these materials at high-temperature. The inhomogeneity might arise from the presence of pores at the metal surface or from microstructural heterogeneity. Therefore, the main aim of this work is to carry out a comparative orderly study on the high temperature oxidation behavior of porous-nickel prepared by conventional powder metallurgy and cast-nickel with microstructural inhomogeneity in air at 1273 K under atmospheric pressure for a total oxidation time of 100 h.

## Experimental

The porous nickel test-samples used in this investigation were fabricated from nearly spherical particles of nickel powder with an average particle size of about 85  $\mu\text{m}$ . Nickel green samples were compacted under 420 MPa and the green samples were then sintered in a vacuum furnace ( $10^{-3}$  torr) at 1473 K for 2 h. Test-specimens were produced as pellets with 18.5–19 mm in diameter and 3.5–3.7 mm in thickness. The obtained samples had an average apparent density of 7.58  $\text{g}/\text{cm}^3$ , and in turn, the average porosity of test-samples was about 14.8%. The average density value for the inhomogeneous cast-nickel samples was measured and found to be 8.6  $\text{g}/\text{cm}^3$ . Thus, its average porosity was estimated to be 3.4%.

The composition of nickel powder and cast-nickel as given by the suppliers and as obtained by wet chemical analysis are listed in Table 1. The composition obtained by wet chemical analysis verified to a great extent the chemical composition given by the suppliers. The data in Table 1 indicates that the total impurity level in the nickel powder is about 0.1% and that of the cast-nickel ranges from 0.1 to 0.2%.

For microstructural examination of test-samples, a pellet of each type of test-samples was mounted and ground successively with silicon carbide abrasive papers with grit size ranging from 100 to 800, and then polished with 0.3  $\mu\text{m}$  alumina paste. The samples were then etched in an aqueous solution consisting of 15  $\text{cm}^3$  nitric acid (70 wt%  $\text{HNO}_3$ +30 wt%  $\text{H}_2\text{O}$ ) and 90  $\text{cm}^3$  acetic acid (99.5 wt%  $\text{CH}_3\text{COOH}$ ) [23]. The microstructure of the etched pellets was observed by optical microscopy using “Olympus BX41M-LED microscope” and scanning electron microscopy (SEM) utilizing “FEI Company, Quanta 250 FEG, made in Netherlands”.

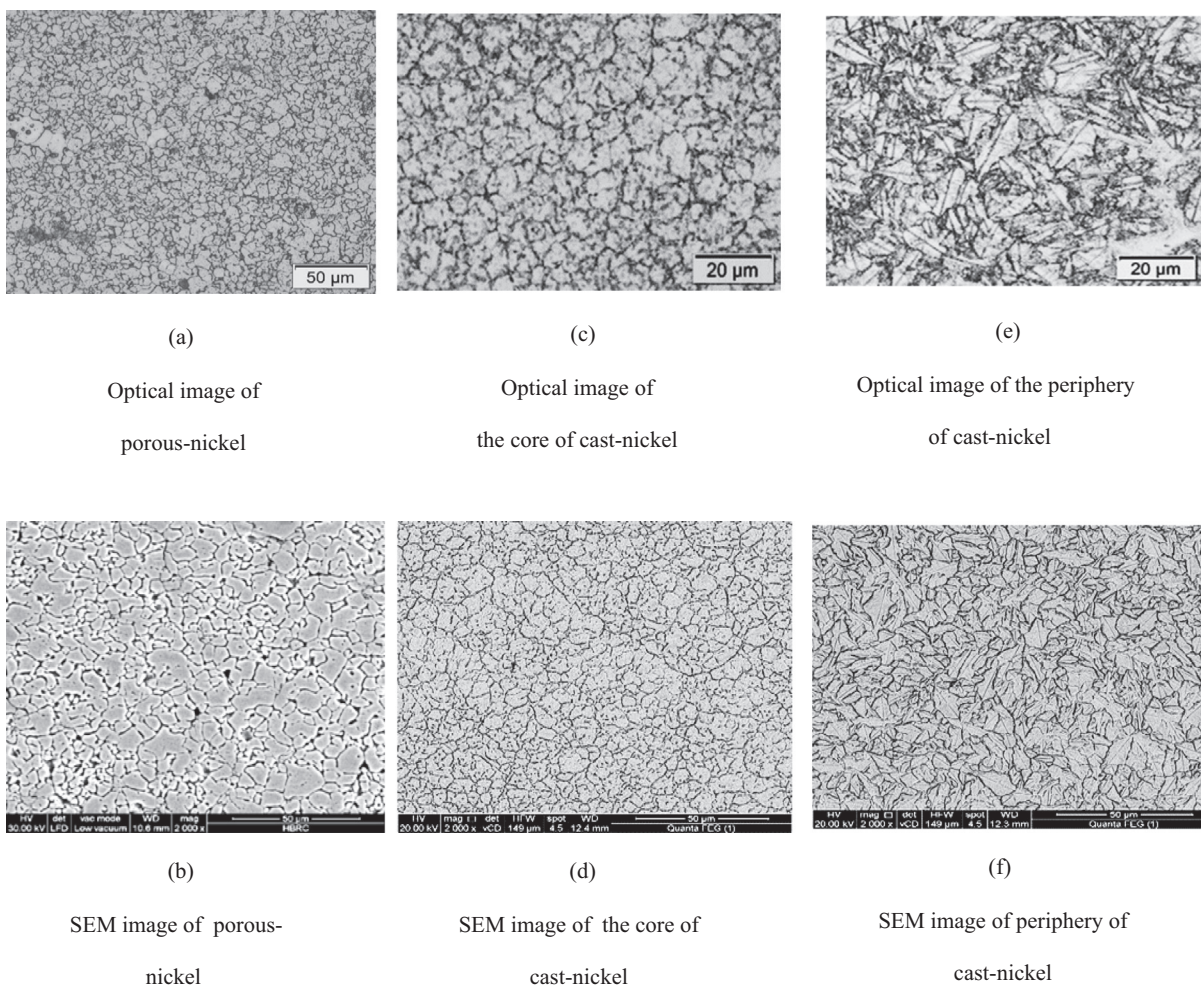
The oxidation kinetics was measured for three porous-nickel samples (1, 2, and 3) and three cast-nickel samples (4, 5, and 6). The measurements were performed for each sample individually to examine the reproducibility of the process. The oxidation kinetics of each sample was carried out in air at 1273 K for a total oxidation time of 100 h. The weight gain per unit area as a function of time for each sample was observed during the oxidation test using the gravimetric method; a microbalance with an accuracy of  $10^{-4}$  g was used in this investigation.

Visual and photographic examinations were conducted to view the macrostructure of the formed oxide scales. Microstructure observations were carried out by using optical microscopy, and scanning electron microscopy (SEM) which was also employed to view the topography of the formed oxide scales. Diffraction patterns of each of the surfaces of the oxidized six samples were obtained using X-ray diffractometry (XRD) using “X’Pert PRO PAN

**Table 1**

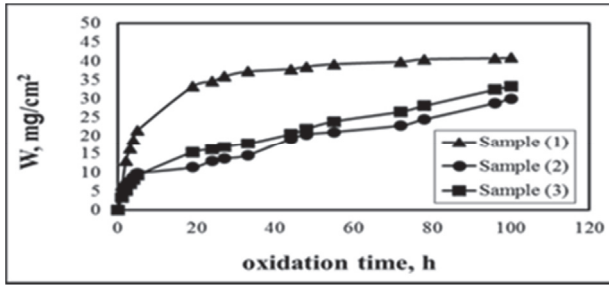
The chemical analysis of nickel powder and cast-nickel samples.

Elements, %	Composition			
	Nickel powder		Cast nickel	
	Given by the supplier <sup>a</sup>	Obtained by wet chemical analysis <sup>c</sup>	Given by the supplier <sup>b</sup>	Obtained by wet chemical analysis <sup>c</sup>
C	0.08	0.07	<0.0035	0.1
S	0.001	N.D.	0.019–0.025	N.D.
Fe	0.01	0.015	–	–
Cu	–	–	<0.0008	0.0001
Zn	–	–	<0.002	N.D.
As	–	–	<0.0015	N.D.
Pb	–	–	<0.0003	0.0002
Co	–	–	<0.065	0.0003
Ni	Bal.	99.9	Bal.	99.83

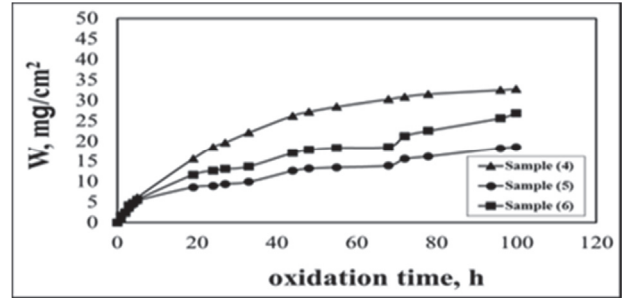
<sup>a</sup> Analysis given by the supplier (Dop. company).<sup>b</sup> Analysis given by the supplier (Vale company of vale™ electrolytic nickel s-rounds).<sup>c</sup> results of the wet chemical analysis in the laboratories of the “Egyptian Mineral Resources Authority (EMRA)”.**Fig. 1.** Optical and SEM images of porous-nickel (a and b), cast-nickel core (c and d), and cast-nickel periphery (e and f) of test-samples.

analytical diffractometer (made in Netherlands, 2007), with Cu  $K\alpha$  radiation- $\lambda = 0.15406$  nm, 45 kV and 40 mA”. X-ray energy dispersive analysis (EDAX) using “FEI Company, Quanta 250 FEG analyzer (Netherlands)” was employed for spot EDAX elemental (O and Ni) analysis and also for having oxygen and nickel profiles along the cross-section of oxidized samples.

For the microstructure examination of the cross-section of the oxidized pellets, each sample was vertically mounted in a mould, and then ground successively with silicon carbide abrasive papers with grit size ranging from 80 to 800 until almost one half of the sample was removed, and then the cross-section was polished with 0.3  $\mu$ m alumina paste.

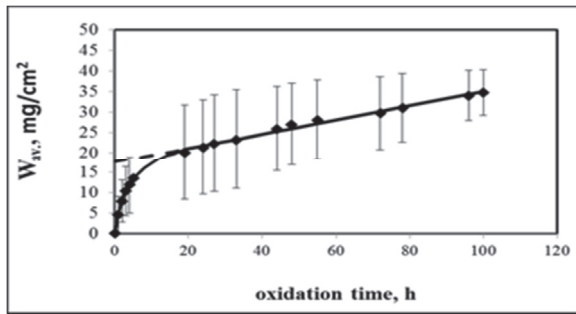


(a) porous-nickel samples

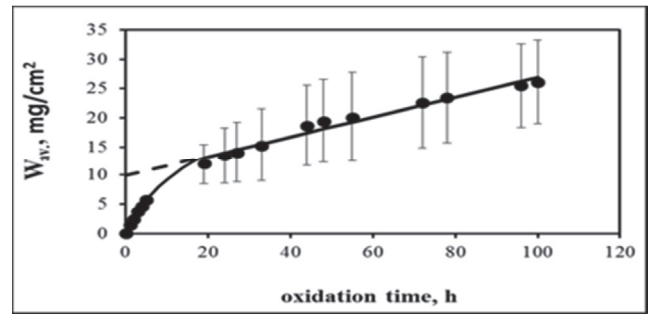


(b) cast-nickel samples

Fig. 2(I) The kinetic curves of the oxidation process of three test-samples of porous-nickel (a) and of cast-nickel (b)



(c) average of Fig. 2(I-a)



(d) average of Fig. 2(I-b)

Fig. 2(II) The dependence of average weight gain on time for the three test-samples of porous-nickel (c) and of cast-nickel (d)

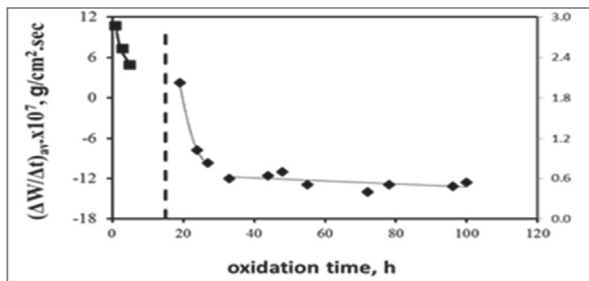
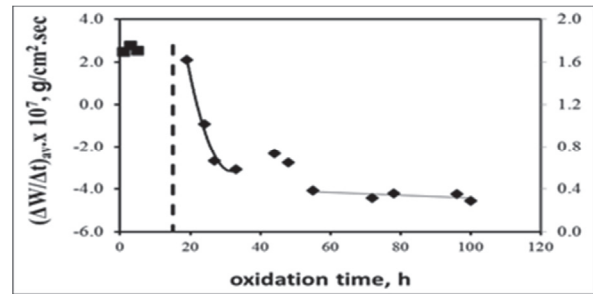
(e) slope  $(\Delta W_{av}/\Delta t)$  of Fig. 2(II-c)(f) slope  $(\Delta W_{av}/\Delta t)$  of Fig. 2(II-d)

Fig. 2(III) The dependence of the average oxidation rate on time for the porous-nickel (e) and for cast-nickel (f)

Fig. 2. The dependence of the weight gain of three test-samples of porous-nickel and three test-samples of cast-nickel on time 2(I), their average weight gain 2(II), and average oxidation rate 2(III) oxidized in air at 1273 K for 100 h.

## Results and discussion

### Microstructure of the metal test-samples

Typical optical and scanning electron images of porous-nickel and cast-nickel (core and periphery) test-samples are shown in Fig. 1, which clearly indicates the formation of pores and triple

points at the grain boundaries of porous-nickel, Fig. 1(a) and (b). The microstructural inhomogeneity of a typical cast-nickel test-sample is also shown in Fig. 1, where equiaxed grains are found at the core, Fig. 1(c) and (d), and elongated grains are formed at the periphery as shown in Fig. 1(e) and (f). Spot EDAX results for porous-nickel and the periphery of the cast-nickel samples indicated the existence of only oxygen and nickel peaks. The oxygen

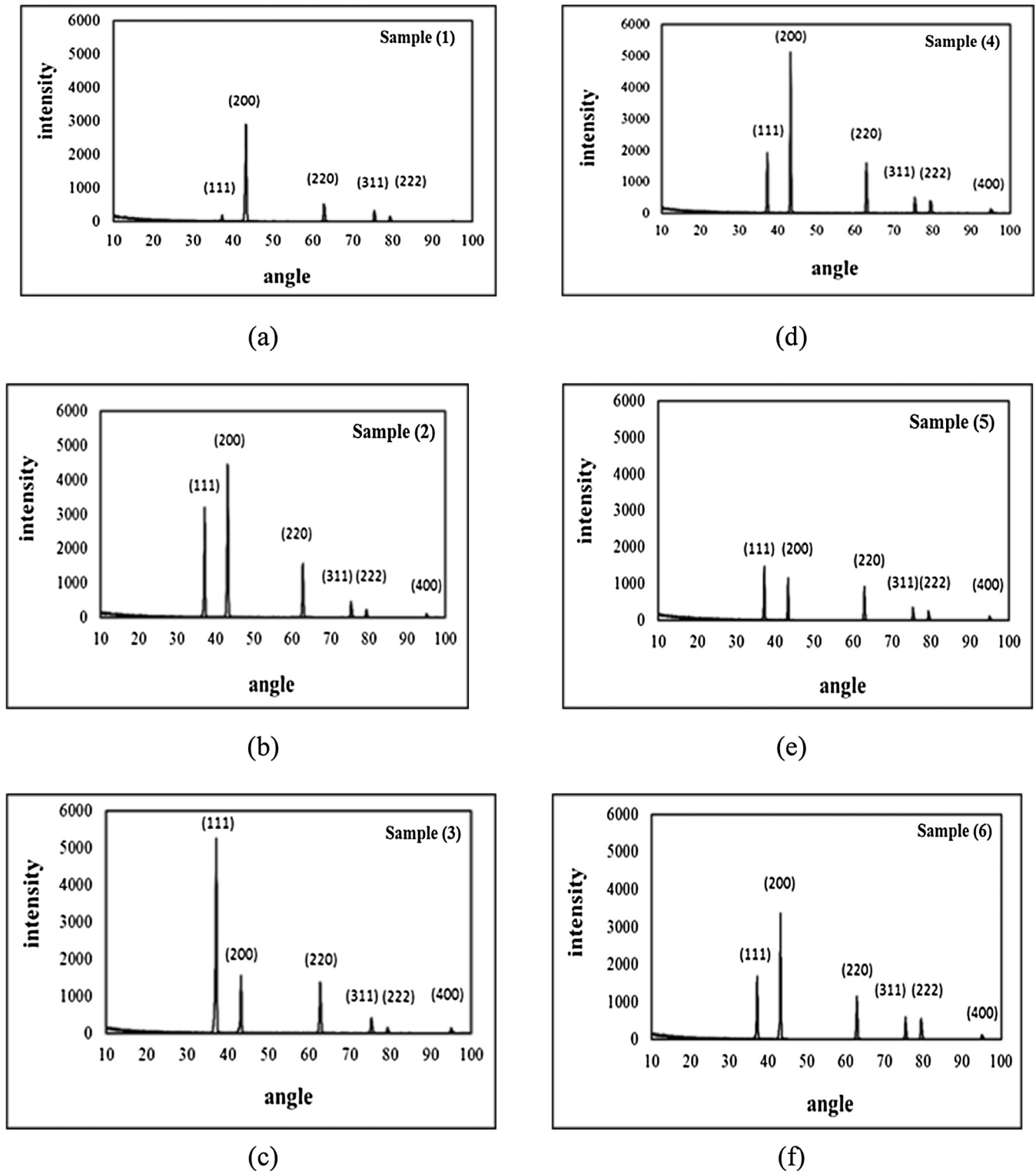


**Fig. 3.** XRD patterns obtained from the surfaces of the oxidized samples of porous-nickel samples (a) sample (1), (b) sample (2), and (c) sample (3) and for the oxidized cast-nickel samples (d) sample (4), (e) sample (5), and (f) sample (6).

percent indicator (OI) at different spots of the porous-nickel samples reached up to 2.64% while the corresponding value at the periphery of cast-nickel samples was about 1%. The spot EDAX results at the cores of cast-nickel samples had no oxygen peaks (a sign of negligible content of oxygen at the core of the cast-samples).

#### Oxidation kinetics

Fig. 2(I) shows the dependence of weight gain per unit area of each of the three test-samples of porous-nickel, Fig. 2(I-a), and each of the three test-samples of cast-nickel, Fig. 2(I-b). All kinetic curves indicated that the oxidation rate was initially rapid and

**Table 2**  
The relative intensity percent of the peaks of the XRD pattern obtained from the surfaces of the six samples and the corresponding peaks reported in literature for NiO powder [25].

Sample No.	Relative intensity percent					
	(1 1 1)	(2 0 0)	(2 2 0)	(3 1 1)	(2 2 2)	(4 0 0)
NiO Powder [25]	68	100	44	14	10	3
Sample 1 (Porous-nickel)	5	100	17	14	2	2
Sample 2 (Porous-nickel)	65	100	35	9	4	41
Sample 3 (Porous-nickel)	100	35	28	8	3	3
Sample 4 (Cast-nickel)	36	100	27	6	3	2
Sample 5 (Cast-nickel)	100	63	56	21	16	8
Sample 6 (Cast-nickel)	58	46	100	32	16	16

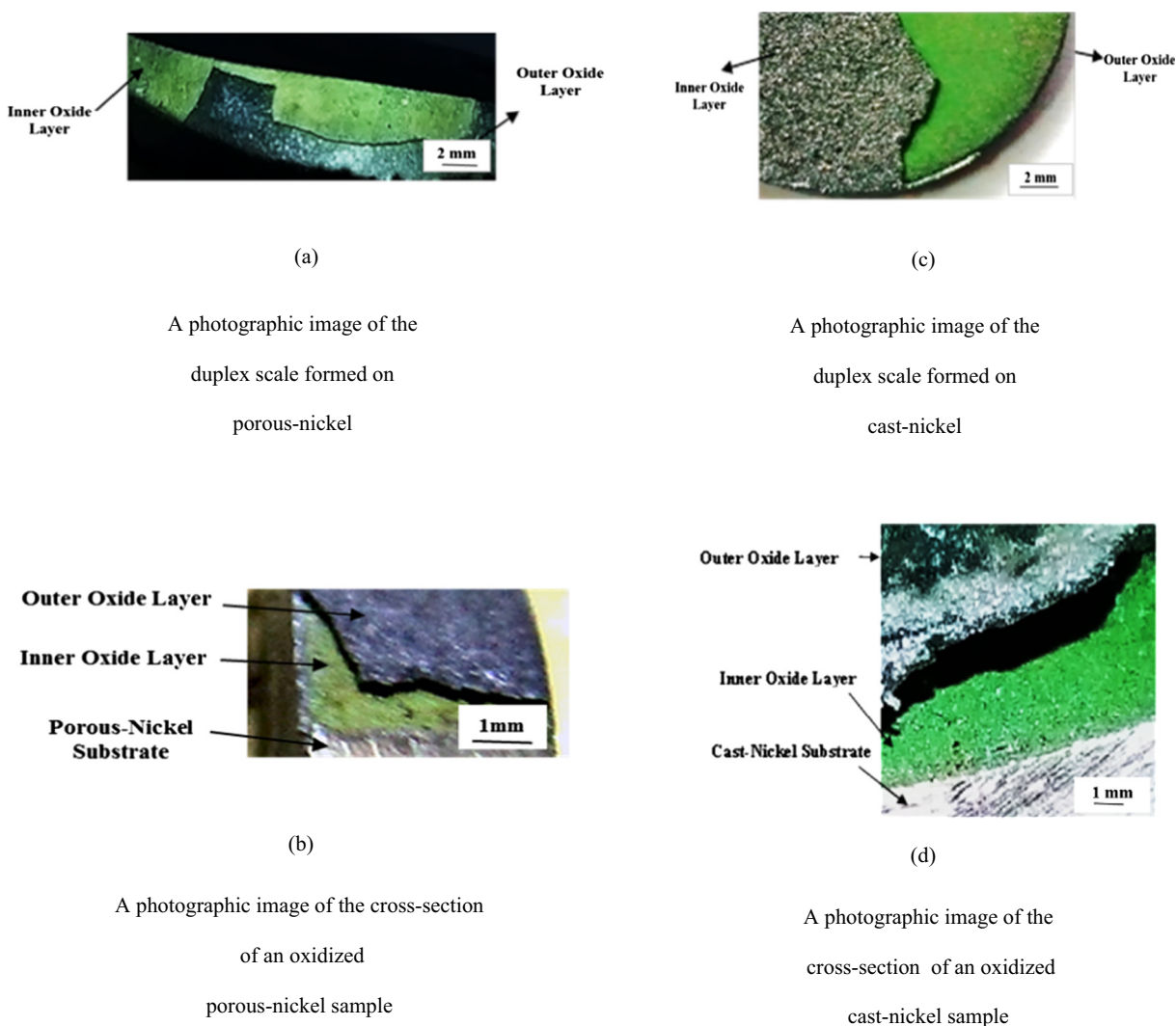
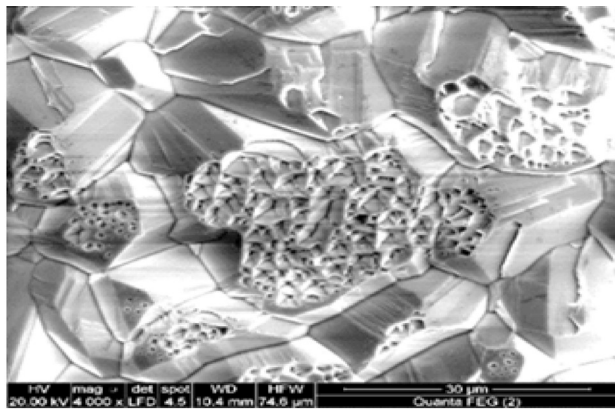


**Fig. 4.** The macrostructure of the duplex oxide scales formed on porous-nickel samples (a and b) and on cast-nickel samples (c and d).

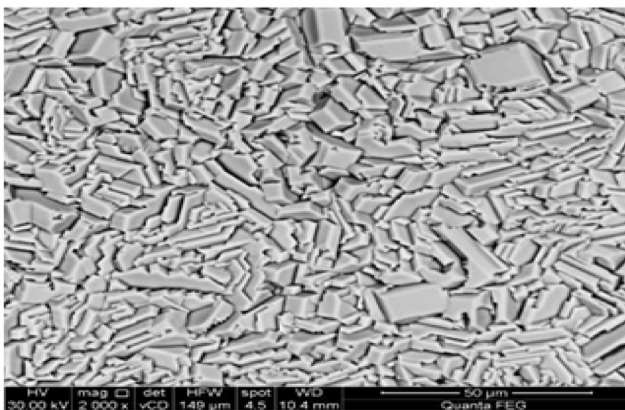
then gradually decreased over a period of about 40 h (transient-stage). Later, a linear rate (steady-state rate) was observed. At some points during the steady-state period, the kinetic rates showed a rapid increase for a short period of time and then it started to slow down again nearly to the steady-state linear rate. This rapid increase might arise from the development of more easy paths which allow molecular oxygen migration such as micro-cracks propagation, cavities development and partial separation of the oxide layers from the metal substrate [8]. These easy paths

for molecular oxygen migration might be due to the development of internal stresses within the oxide scales [8].

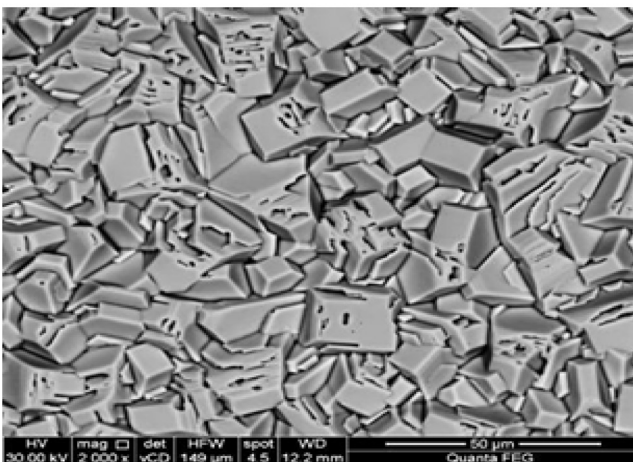
The dependence of the average weight gain per unit area on time is shown in Fig. 2(II). The average weight gain per unit area for the three porous- and also for the three cast-nickel samples are plotted in Fig. 2(II-c) and (II-d), respectively. Both Figures were found to behave linearly after about 40 h for the rest of the oxidation process. The bars shown in the figures represent the standard deviation at each point. The highest value of the standard deviation for the aver-



(a)



(b)

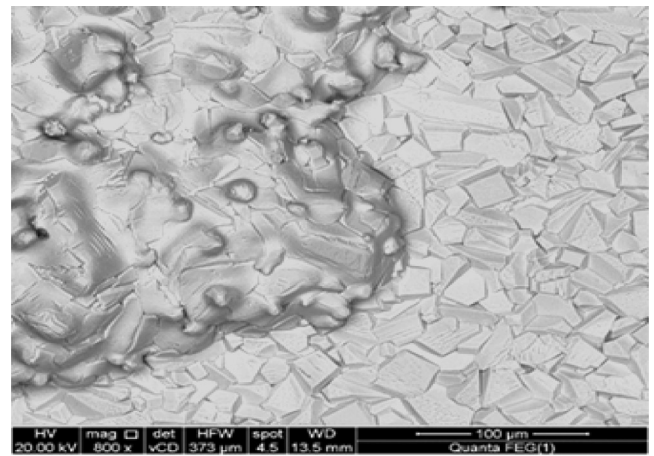


(c)

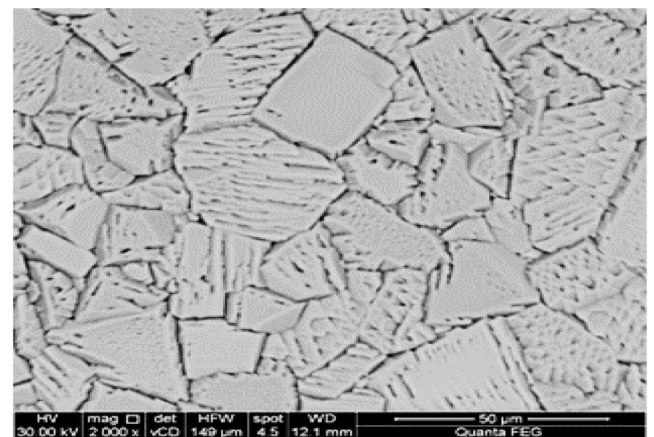
**Fig. 5.** SEM images for the surfaces of the oxidized porous-nickel test-samples of (a) sample (1), (b) sample (2) and (c) sample (3).

age weight gain per unit area of the porous-nickel samples was  $\pm 58\%$  and the corresponding value for the cast-nickel samples was  $\pm 41\%$ . This, in turn, might be caused by the higher inhomogeneity of the porous-nickel samples than that of the cast-nickel samples.

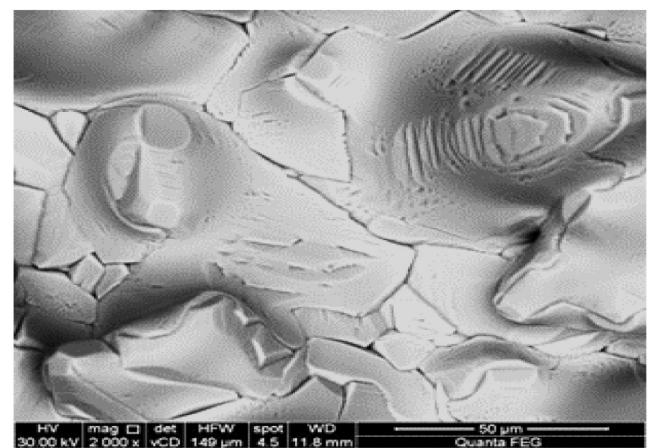
The dependence of the average rate of oxidation on time is shown in Fig. 2(III). The average rate of oxidation is estimated by using the relation  $\Delta W_{av}/\Delta t$  where  $\Delta W_{av}$  is given by the change in average weight gain per unit area over the time period  $\Delta t$ . The



(a)



(b)



(c)

**Fig. 6.** SEM images for the surfaces of oxidized three cast-nickel test-samples of (a) sample (4), (b) sample (5) and (c) sample (6).

dependence of the average oxidation rate for porous- and cast-nickel is shown in Fig. 2(III-e) and (III-f), respectively. It is clear from all Figures that the growth rate of the oxide scales at the initial stage is rapid and then it slows down until it reaches a constant value (linear behavior). The values of the linear rate constants were about  $5.5 \times 10^{-8} \text{ g/cm}^2 \text{ s}$  and  $3.4 \times 10^{-8} \text{ g/cm}^2 \text{ s}$  for porous- and

cast-nickel, respectively, which means a better oxidation resistance of cast-nickel than porous-nickel.

#### Texture analysis of the outer oxide layers

The diffraction patterns, Fig. 3, obtained from the surfaces of the oxidized samples, under the oxidation conditions used in this work, confirmed that  $\text{Ni}_{1-x}\text{O}$  is the only oxide phase formed which is in agreement with literature [1,24]. Accordingly, the relative intensity percent of the peaks of the XRD pattern obtained from each of the surfaces of the oxidized samples might reflect the texture of each of the outer oxide layer.

Fig. 3 shows the XRD patterns obtained from the outer surfaces of the oxide scales formed on the six nickel samples (three porous and three cast). The obtained peaks coincided with the peaks reported for nickel oxide powder in literature [25].

The relative intensity percent of the obtained peaks of the six patterns obtained from the surfaces for the test-samples and the corresponding peaks reported for  $\text{NiO}$  powder in literature [25] are listed in Table 2. These data indicated that the oxide grains in the outer oxide layers of the scales might have crystallographic (1 1 1), (2 0 0), and (2 2 0) preferred orientation for samples (3 and 5), (1 and 4) and 6, respectively. This preferred orientation might refer to the formation of columnar grains at the outer part of the oxide scales.

#### Macrostructure of the oxide layers

Fig. 4 shows the macrostructure of the duplex oxide scales formed on a porous- sample and on a cast-nickel test-sample as detected by visual examination. Fig. 4(a) and (b) show that the color of the outer oxide layer formed on a porous-nickel sample is black with glossy and dark parts, and the color of the inner layer is light green. The two oxide layers formed on the cast-nickel samples are shown in Fig. 4(c) and (d). The outer one had a dull greenish-black color, while the color of the inner oxide layer was light green. The formation of colored-duplex scale is reported in previous work [24]. The molecular oxygen inward migration leads to the formation of  $\text{NiO}$  duplex scales [21,22], which are generally composed of small equiaxed grains at the metal/oxide interface overgrown by larger columnar grains in the external part, the duplex scales are generally formed at temperatures less than 1273 K [8].

#### Surface topography and microstructure of the oxidized nickel samples

Fig. 5 shows the surface topography observed by SEM for the oxide scales formed on the three porous-nickel samples 1, 2, and 3, as shown in Fig. 5(a)–(c), respectively. The surface topography of the porous-nickel samples shows a dimpled structure surrounded by cleavage zones, Fig. 5(a), faceted structure, Fig. 5(b), and pores within the nickel oxide grains, Fig. 5(c), which might have acted as nuclei for the dimples. Fig. 6(a)–(c) also show the topography observed by SEM for the surfaces of oxide scales formed on the three cast-nickel samples 4, 5, and 6, respectively. The presence of faceted structure and parallel microfissures across some grains (the parallel directions differ from one grain to another) is revealed from Fig. 6(a) and (b). Moreover, pores are detected within the grains on the surfaces of these scales, Fig. 6(c).

The EDAX results obtained at different spots of the mentioned surfaces showed that the OI varied from about 6% to 18%. This variation might be caused by the porosity of the scale and the unevenness of the surfaces of the oxide scales.

Figs. 7 and 8 illustrate the microstructures of the cross-sections of the oxidized porous- and cast-nickel samples. Fig. 7(a) and (b) show the optical images of the porous- and cast-nickel samples,

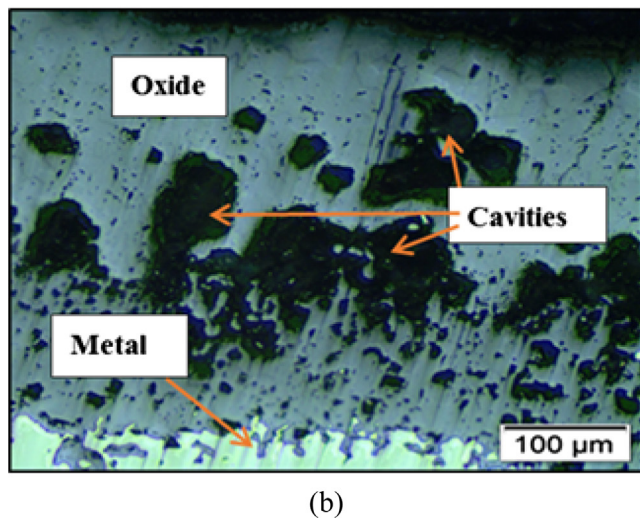
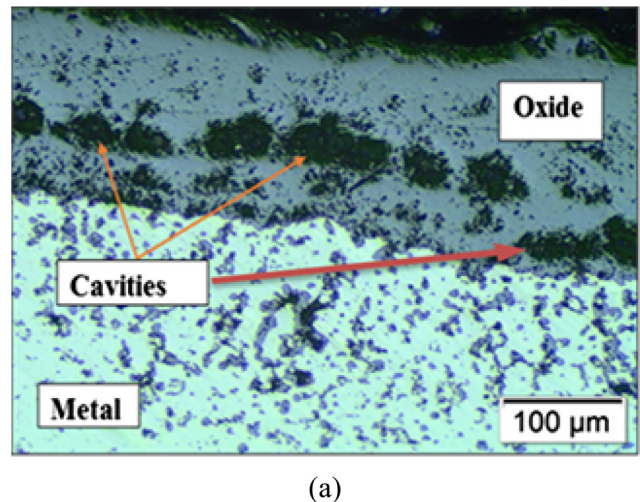
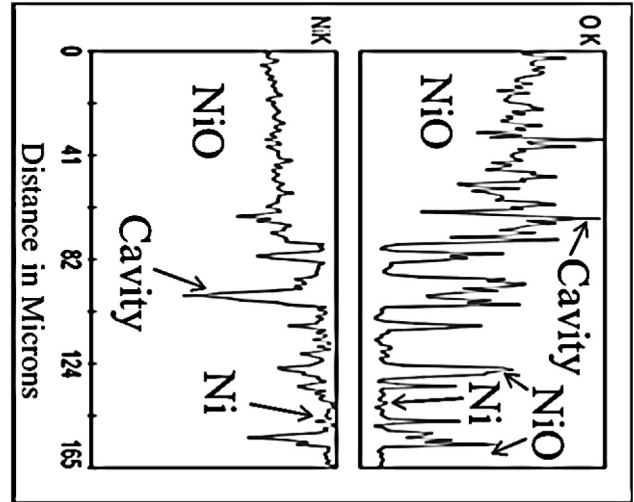
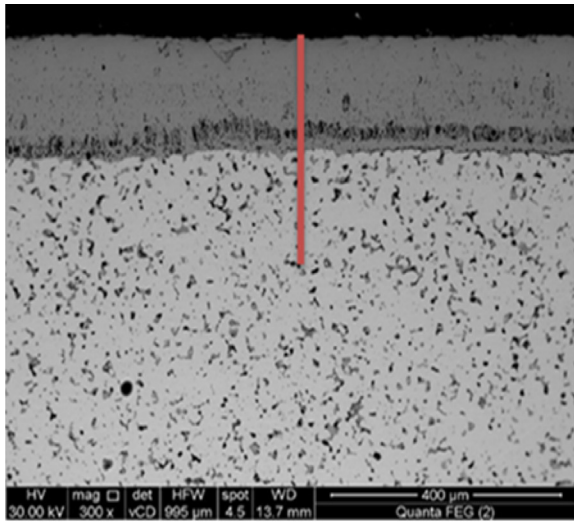


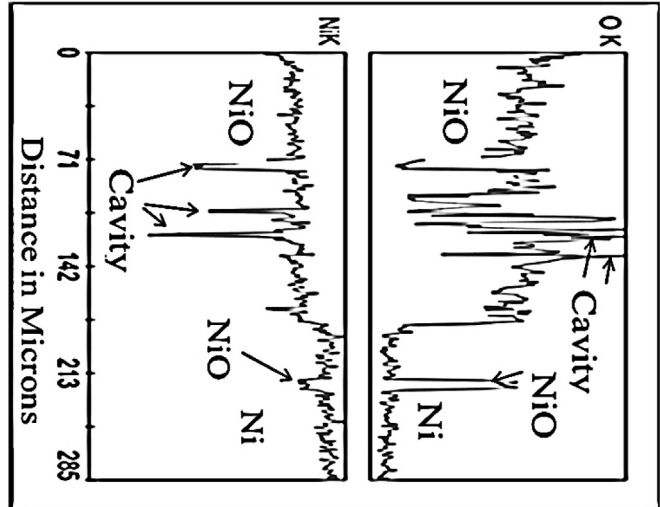
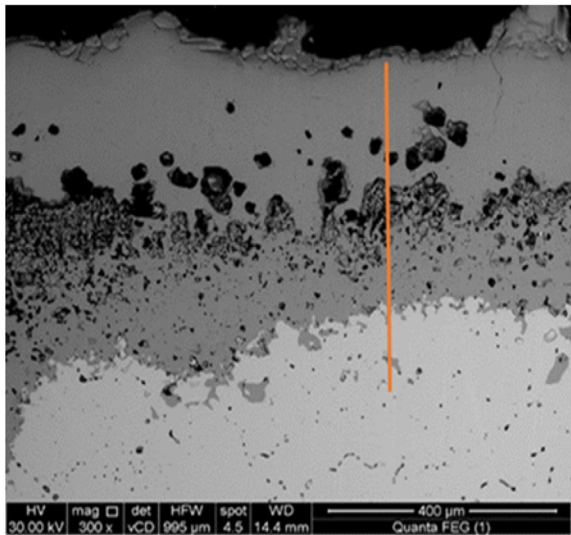
Fig. 7. Optical images of the cross-sections of oxidized porous-nickel test-sample (a) and cast-nickel test-sample (b).

respectively; whereas Fig. 8(a) and (b) show the SEM images and the corresponding oxygen and nickel line-profiles for the oxidized porous- and cast-nickel samples, respectively. The optical and SEM Figures indicated that oxide duplex scales were developed on the porous- and cast-nickel test-samples. The two layers were partially separated from each other because of the formation of cavities between the two layers. In some parts, the lower layer (about 50  $\mu\text{m}$  in thickness) was overgrown by an upper layer (about 100  $\mu\text{m}$  in thickness). In other parts, the lower layer was noticed to be less than 10% of the thickness of the upper layer. The two oxide layers of the duplex scale were noticeably porous.

The nickel and oxygen line-profiles recorded along the cross-section of the oxidized samples are also shown in Fig. 8. It was noticed that the oxygen profile was high along the oxide scale and that it decreased to an almost very low level along the metal phase region; while the nickel profile was observed to have its highest level over the metal phase region. The oxygen profile increased over cavities to its highest value because these cavities were filled with air. Also, if a closed pore was just underneath the surface layer, both oxygen and nickel profiles would simultaneously get lower. The EDAX profiles in Fig. 8 also indicate the formation of  $\text{NiO}$  particles within the pores of the porous-nickel samples; since repeated peaks of oxygen are observed on the oxygen profile and these oxygen peaks are associated with decrease in the nickel profile.



(a)



(b)

Fig. 8. SEM images and line EDAX profiles for oxygen and nickel along the cross-sections of oxidized porous-nickel test-sample (a) and cast-nickel test-sample (b).

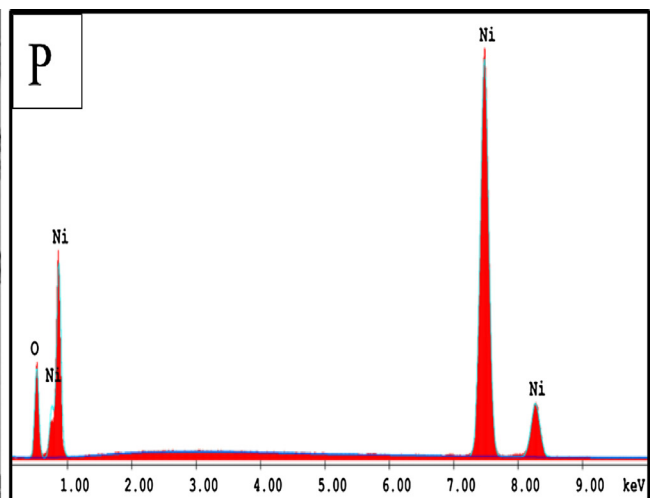
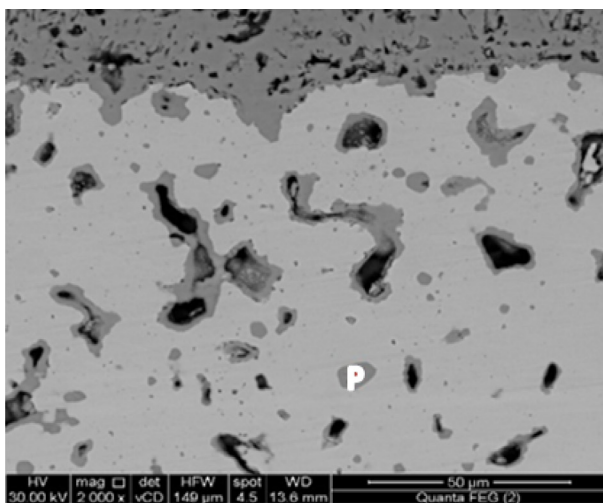


Fig. 9. SEM image for the porous-nickel substrate and EDAX results for a NiO particle formed inside one of the pores (p).

Fig. 9 shows an SEM image and the corresponding spot EDAX results on a particle developed at one of the sample pores (P). The spot EDAX results yielded only Ni and O peaks which, in turn, indicated the formation of NiO particles.

SEM images of the cross-sections of the cast-nickel samples before and after oxidation are shown in Fig. 10. The images indicate the formation of voids within the metallic phase after oxidation; this phenomenon is previously reported in literature [26]. The size of these voids decreased with the depth in the metallic phase measured from the scale/metal interface. The density number of these voids was also decreasing with that depth until they nearly vanished. The SEM image in Fig. 10 indicates that the cast-nickel samples were almost free from porosity before oxidation, as shown in Fig. 10(a). The formation of voids within the metallic phase is revealed from Fig. 10(b).

The OI of the outer oxide layer formed on porous-nickel samples was 11.56% and almost the same value was detected for the inner oxide layer while a value of about 1.5% for the OI was

obtained in the metal substrate. As for the cast-nickel, the OI of the outer oxide layer is about 11.54% and almost the same value was obtained for the inner oxide layer while a value of 0.85% was detected for the OI of the metal phase.

The volume fraction percent of the voids decreases with the increase in depth, below the scale/metal interface of the oxidized cast-nickel test-sample as shown in Fig. 11 which also shows the high volume fraction of the pores developed within the oxide scale formed on the metal substrate. The high values of the volume fraction of the pores at the surface of the oxide scale revealed that the pores were initially nucleated at the surfaces of the oxidized samples; while the highest value of the volume fraction was developed at the scale/metal interface. This could be mainly related to the formation of cavities at the scale/metal interface; which is attributed to the loss of adherence at the oxide/metal interface resulting from the development of internal stresses [5,8].

Adherent and protective nickel oxide scales are formed on pure-homogenous nickel substrates upon oxidation in air (or oxygen) at

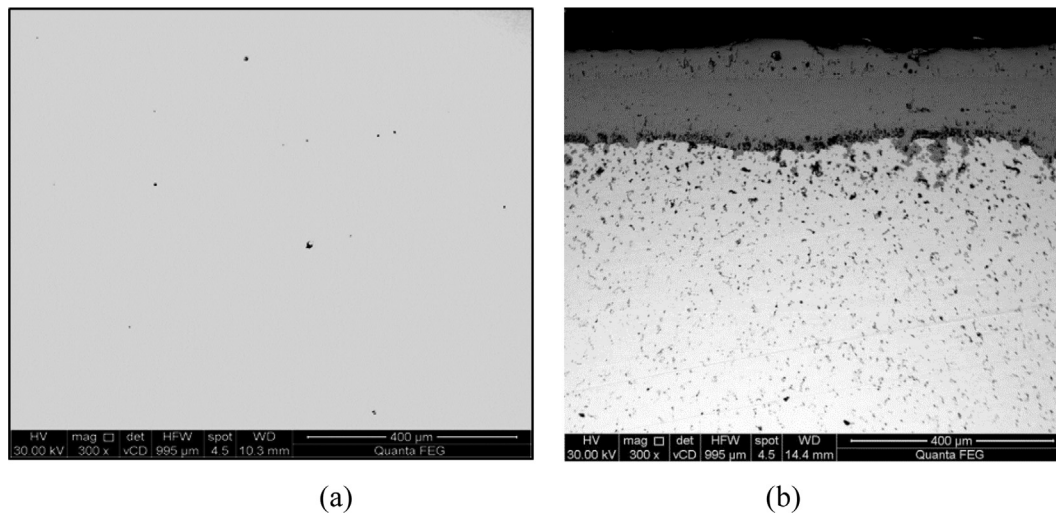


Fig. 10. SEM images of the cross-section of a cast-nickel sample before oxidation (a) and after oxidation (b).

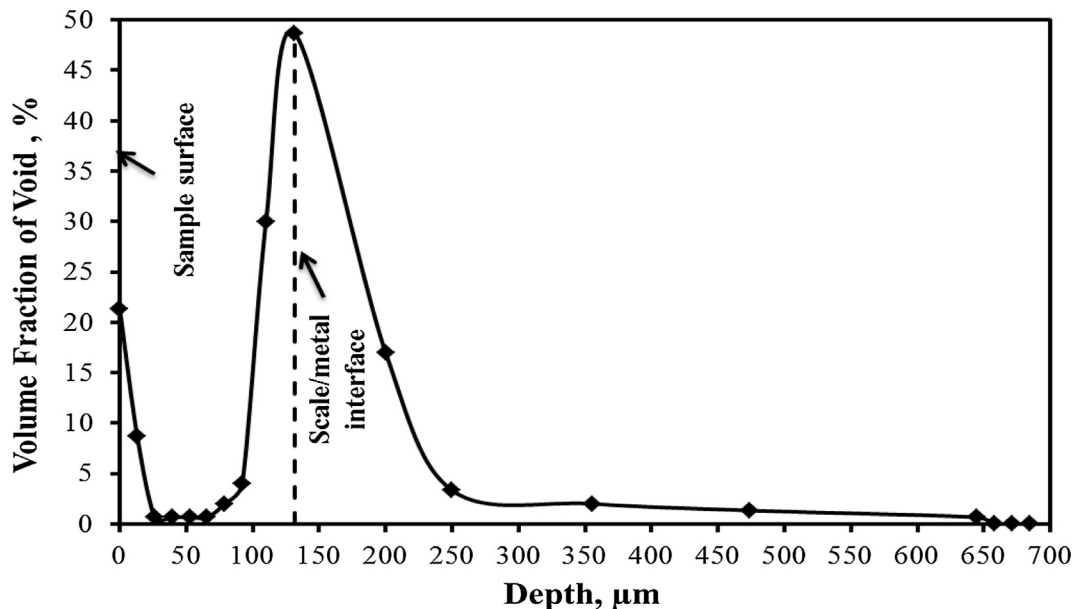


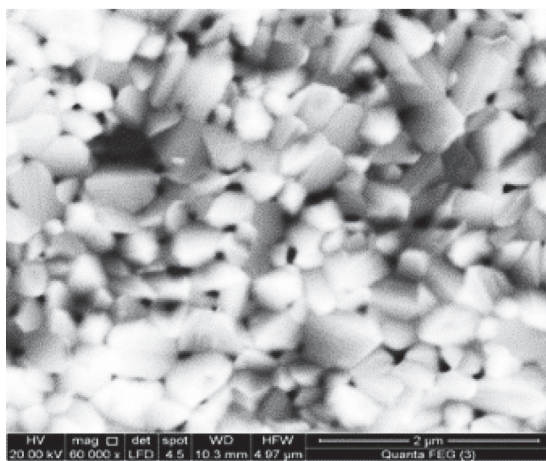
Fig. 11. The percentage of the volume fraction of voids with the depth below the oxidized cast-nickel sample surface of Fig. 10(b).

1273 K [11,24]. The scales are grown by outward cationic lattice diffusion [6,11,24]. The average parabolic rate constant of the oxidation process of nickel under these conditions is about  $3.5 \times 10^{-11} \text{ g}^2/\text{cm}^4 \text{ s}$ . Accordingly, the thickness of the NiO layer formed in this case is about  $35 \mu\text{m}$  which is 4–5 times smaller than the thickness of the oxide layer, about  $150 \mu\text{m}$ , formed on the inhomogeneous cast-nickel used in this work. Moreover, the depth of the metal substrate region containing voids detected in this work is found to be about  $130 \mu\text{m}$ ; which is not observed in the case of oxidation of sound-homogenous pure nickel [11].

#### Oxidation mechanism

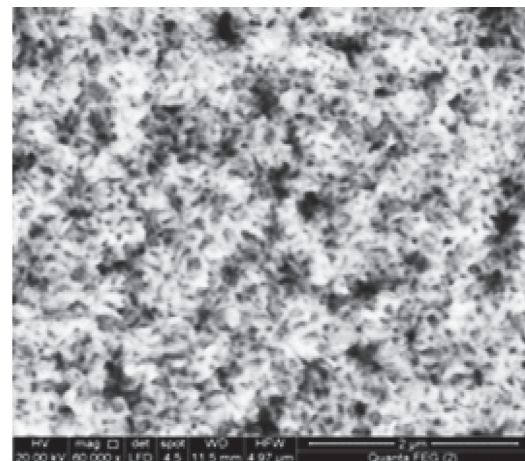
Fig. 12 shows the topography of initially formed oxides on porous- and cast-nickel samples observed by SEM after oxidation time of 10 and 30 min. Fig. 13 also illustrates the microstructure

of the cross-sections of oxidized porous- and cast-nickel samples noticed by SEM after 10 and 30 min oxidation time. Fig. 12 (a) and (c) indicate the formation of a highly porous oxide layer on the porous-nickel samples oxidized for 10 and 30 min, respectively, while Fig. 12(b) and (d) show the buildup of a network of ridges with a cellular appearance of NiO layer on the cast-nickel samples which were oxidized for 10 and 30 min, respectively. The cross-section images also indicate the formation of a discontinuous thin layer on the porous-nickel test-samples, as shown in Fig. 13(a) and (c), and the formation of NiO particles within the pores of the porous-nickel test-samples. Microcracks propagation extending from the pores of porous test-samples through the metal matrix was, also, noticed. This, in turn, might be due to the acting internal stresses which could be induced by the NiO particles formed within the pores. Microcracks were also observed to extend from the NiO layer formed on the surface of the porous-nickel



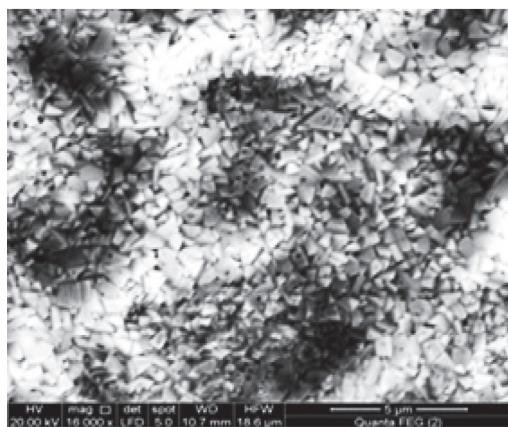
(a)

Surface topography, 10 min  
oxygen% indicator = 13.26



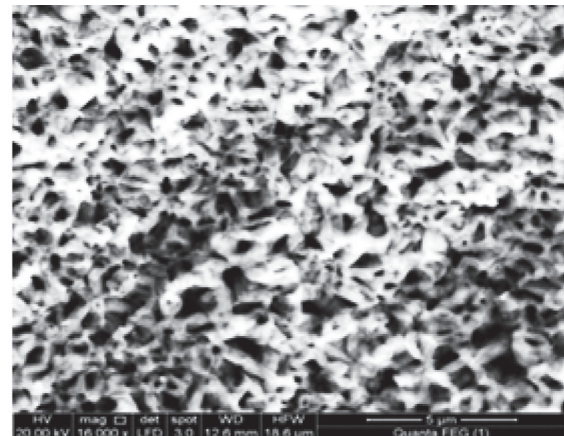
(b)

Surface topography, 10 min  
oxygen% indicator = 4.36



(c)

Surface topography, 30 min  
oxygen% indicator = 14.08



(d)

Surface topography, 30 min  
oxygen% indicator = 12.78

**Fig. 12.** SEM images of the surface topography of the oxidized samples for 10 and 30 min formed on the porous-nickel samples (a and c) and the cast-nickel samples for 10 and 30 min (b and d).

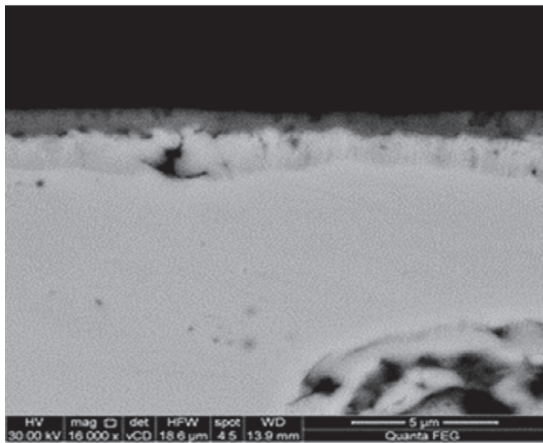
test-samples to the inner metal phase region. Fig. 13(b) and (d) indicate the formation of fragile NiO layers on the cast-nickel test-samples. The formation of a highly porous single layer on both cases indicated that the oxidation mechanism at the initial oxidation period was controlled by inward migration of molecular oxygen.

The values of OI detected by spot EDAX analysis were 13.2% and 14.08% for the thin layers formed on the porous-nickel samples after 10 and 30 min, respectively. The corresponding values for cast-nickel were 4.36% and 12.78%; this might be due to the discontinuity of the thin layers and the ridge structure of this oxide layer which was formed on the cast-nickel after 10 min of oxidation.

After about 40 h of oxidation, steady-state conditions (linear oxidation rate) started to dominate the growth rate of the oxide scales and the scales were observed to be of duplex nature.

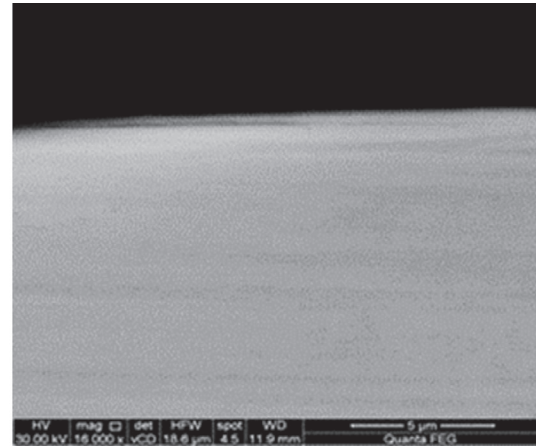
The formation of a duplex scale might be initiated by loss of adherence between the single layer and the metal substrate due to the buildup of internal stresses within the oxide scale giving the possibility of formation of a second layer between the upper oxide layer and the metal substrate.

The linear kinetics, the topography of the oxide scales which revealed the formation of paths for molecular oxygen migration, the duplex-porous scale, the formation of cavities and formation of NiO particles within the pores of the porous-nickel samples, all indicate the growth of oxide scales by inward migration of molecular oxygen along the NiO scale [1,8,21,22]. The oxygen molecules might also migrate through the open pores of the porous-nickel samples forming NiO particles within these pores. On the other hand, most of the voids formed within the matrix of the cast-nickel samples, which were relatively smaller than the pores of the porous-nickel, did not include NiO grains.



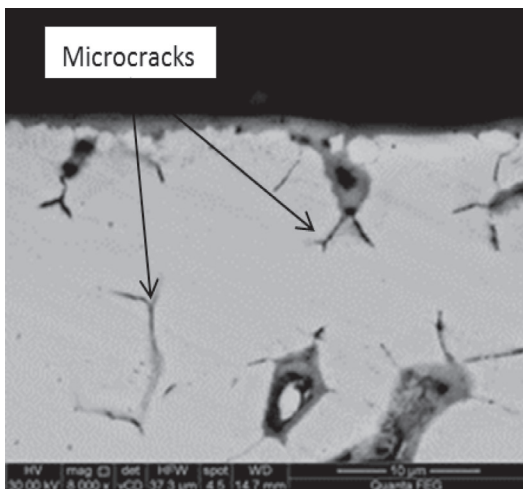
(a)

10 min



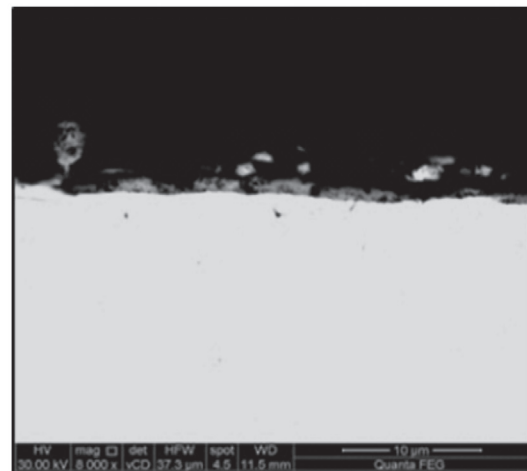
(b)

10 min



(c)

30 min



(d)

30 min

Fig. 13. SEM images of the cross-section of the oxidized samples for 10 and 30 min formed on the porous-nickel samples (a and c) and the cast-nickel samples (c and d).

Accordingly, the oxidation mechanism based on inward migration of molecular oxygen through the NiO duplex-scale should be the main mechanism for the oxidation process of inhomogeneous nickel substrates. The formation of the voids within the metallic phase of the cast-nickel might be explained on the basis of annihilation of vacancies formed at the oxide/metal interface in the metal phase lattice as previously reported [26].

## Conclusions

The oxidation behavior of two types of inhomogeneous nickel is systematically investigated. The oxidation rate for both types is initially rapid and then it gradually decreases with time to a constant rate which is attained after about 40 h. The linear rate constants are about  $5.5 \times 10^{-8}$  g/cm<sup>2</sup> s for the porous-nickel type (porosity 14.8%) and  $3.4 \times 10^{-8}$  g/cm<sup>2</sup> s for the cast-nickel type. Initially single thin porous NiO layers are formed on the surfaces of the test-samples of both types. The single layers then change to duplex scales. The two layers of the duplex scales, in general, have two different colors and both are porous. Cavities are formed between the two layers and also at the scale/metal interface. Therefore, the two layers do not adhere to each other; in addition the oxide scale is partially separated from the metal phase. Nickel oxide particles are formed in most of the pores of the porous-nickel substrate. The cast-nickel type shows voids formation in the metal phase whose size and distribution number decrease with depth, measured from the scale/metal interface. In other words, the voids volume fraction decreases with depth. The topography views of the upper surfaces of the NiO scale indicate the formation of easy paths for downwards migration of molecular oxygen. The easy paths include pores, microfissures, dimples and transgranular microcracks. All these observations reveal that the scale growth occurs by inward migration of molecular oxygen; therefore, the newly formed oxide layers take place at the scale/metal interface.

## Conflict of Interest

*The authors have declared no conflict of interest.*

## Compliance with Ethics Requirements

*This article does not contain any studies with human or animal subjects.*

## References

- [1] Atkinson HV. A review of the role of short-circuit diffusion in the oxidation of nickel, chromium, and nickel-chromium alloys. *Oxid Met* 1985;24(3/4):177–97.

- [2] Neil B, Gerald HM, Fred SP. Introduction to the high-temperature oxidation of metals. 2nd ed; 2006. p. 46–8.
- [3] Ahmed JH. Study of optical and electrical properties of nickel oxide (NiO) thin films deposited by using a spray pyrolysis technique. *J Mod Phys* 2014;5:2184–91.
- [4] Saric I, Peter R, Kavre I, Badovinac IJ, Petravic L. Oxidation of nickel surfaces by low energy ion bombardment. *Nucl Instr Meth Phys Res B* 2016;371:286–9.
- [5] Zhou CH, Ma HT, Wang L. Comparative study of oxidation kinetics for pure nickel oxidized under tensile and compressive stress. *Corr Sci* 2010;52:210–5.
- [6] Haugsrud R. On the high-temperature oxidation of nickel. *Corr Sci* 2003;45:211–35.
- [7] Jeangros Q, Hansen TW, Wagner JB, Dunin-Borkowski RE, Hebert C, Herle JV, et al. Oxidation mechanism of nickel particles studied in an environmental transmission electron microscope. *Acta Mater* 2014;67:362–72.
- [8] Chevalier S, Desserrey F, Larpin JP. Oxygen transport during the high temperature oxidation of pure nickel. *Oxid Met* 2005;64(314):219–34.
- [9] Huntz AM, Lefevre B, Cassino F. Roughness and oxidation: application to NiO growth on Ni at 800°C. *Mater Sci Eng A* 2000;290:190–7.
- [10] Unutulmazsoy Y, Merkle R, Fischer D, Mannhart J, Maier J. The oxidation kinetics of thin nickel films between 250 and 500 °C. *Phys Chem Chem Phys* 2017;19:9045–52.
- [11] Elrefaie FA, Manolescu A, Smeltzer WW. Oxidation properties of nickel in the temperature range 1073–1500 K. *J Electrochem Soc* 1985;132(10):2489–93.
- [12] Gulbransen EA, Andrew KF. The kinetics of oxidation of high purity nickel. *J Electrochem Soc* 1954;101(3):128–40.
- [13] Cabanas-Polo S, Bermejo R, Ferrari B, Sanchez-Herencia AJ. Ni–NiO composites obtained by controlled oxidation of green compacts. *Corros Sci* 2012;55:172–9.
- [14] CzeMrinski F. The growth and structure of thin oxide films on nickel superficially modified with ceria and cerium. PhD McGill University. Montreal; 1997.
- [15] Peraldi R, Monceau D, Pieraggi B. Correlations between growth kinetics and microstructure for scales formed by high-temperature oxidation of pure nickel. II. Growth kinetics. *Oxid Met* 2002;58:275–95.
- [16] Nairong S, Lanting Z, Zhigang L, Feng S, Xianping D, Aidang S. The effect of surface machining on the high-temperature oxidation of a single crystal Ni-based superalloy. *Mater Trans* 2014;55(10):1540–6.
- [17] Caplan D, Graham MJ, Cohen M. Effect of cold work on the oxidation of nickel at high temperature. *J Electrochem Soc* 1972;119(9):1205–15.
- [18] Louis PB, Megan F. Effects of crystallographic orientation on the early stages of oxidation in nickel and chromium. *J Mater Sci* 2010;45:1663–71.
- [19] Young DJ. High temperature oxidation and corrosion of metals. 2nd ed.; 2016. p. 85.
- [20] Atkinson A, Smart DW. Transport of nickel and oxygen during the oxidation of nickel and dilute nickel/chromium alloy. *J Electrochem Soc* 1988;135(11):2886–93.
- [21] Kofstad P. On the formation of porosity and microchannels in growing scales. *Oxid Met* 1985;24(5/6):265–76.
- [22] Mrowec S. On the mechanism of high temperature oxidation of metals and alloys. *Corr Sci* 1967;7:563–78.
- [23] John CL, Samuel DK. Welding metallurgy and weldability of nickel-base alloys; 2009. p. 420.
- [24] Gordon EZ. Some high temperature oxidation characteristics of nickel with chromium additions. Project Designation NR 031-355. California Institute of Technology; 1956.
- [25] Taylor D. Thermal expansion data. I. Binary oxides with the sodium chloride and wurtzite structures. *MO Brit Ceram Trans J* 1984; 83: 5.
- [26] Simon P, Bernard V, Daniel M, Laurence R, Eric A. Injection of vacancies at metal grain boundaries during the oxidation of nickel. *Acta Mater* 2004;52(18):5375–80.